Robust expected improvement for Bayesian optimization

Ryan B. Christianson*

Robert B. Gramacy[†]

February 20, 2023

Abstract

Bayesian Optimization (BO) links Gaussian Process (GP) surrogates with sequential design toward optimizing expensive-to-evaluate black-box functions. Example design heuristics, or so-called acquisition functions, like expected improvement (EI), balance exploration and exploitation to furnish global solutions under stringent evaluation budgets. However, they fall short when solving for robust optima, meaning a preference for solutions in a wider domain of attraction. Robust solutions are useful when inputs are imprecisely specified, or where a series of solutions is desired. A common mathematical programming technique in such settings involves an adversarial objective, biasing a local solver away from "sharp" troughs. Here we propose a surrogate modeling and active learning technique called robust expected improvement (REI) that ports adversarial methodology into the BO/GP framework. After describing the methods, we illustrate and draw comparisons to several competitors on benchmark synthetic and real problems of varying complexity.

Keywords: Robust Optimization; Gaussian Process; Active Learning; Sequential Design

1 Introduction

Globally optimizing a black-box function f, finding

$$x^* = \underset{x \in [0,1]^d}{\operatorname{argmin}} \ f(x), \tag{1}$$

is a common problem in recommender systems (Vanchinathan et al., 2014), hyperparameter tuning (Snoek et al., 2012), inventory management (Hong and Nelson, 2006), and engineering (Randall et al., 1981). Here we explore a robot pushing problem (Kaelbling and Lozano-Perez, 2017). In such settings, f is an expensive to evaluate computer simulation, so one must carefully design an experiment to effectively learn the function (Sacks et al., 1989) and isolate its local or global minima. Optimization via modeling and design has a rich history in statistics (Box and Draper, 2007; Myers et al., 2016). Its modern instantiation is known as Bayesian optimization (BO; Mockus et al., 1978).

In BO, one fits a flexible, non-linear and nonparametric response-surface model to a limited campaign of example runs, obtaining a so-called surrogate \hat{f} (Gramacy, 2020). Based on that fit – and in particular its predictive equations describing uncertainty for f(x) at new locations x – one then devises a criteria, a so-called acquisition function (Shahriari et al., 2016), targeting desirable qualities, such as x^* that minimize f. One must choose an surrogate family for f, pair it with a fitting scheme for \hat{f} , and choose a criteria to solve for acquisitions. BO is an example of active learning (AL) where one attempts to sustain a virtuous cycle of learning and data collection. Many good solutions exist in this context, and we shall not provide an in-depth review here.

^{*}Corresponding author: Department of Statistics, Virginia Tech, rchristianson@vt.edu

[†]Department of Statistics, Virginia Tech

Perhaps the most common surrogate for BO is the Gaussian Process (GP; Sacks et al., 1989). For a modern review, see Rasmussen and Williams (2006) or Gramacy (2020). The most popular acquisition function is *expected improvement (EI)* (Jones et al., 1998). EI balances exploration and exploitation by suggesting locations with either high variance or low mean, or both. Greater detail is provided in Section 3.2. EI is highly effective and has desirable theoretical properties.

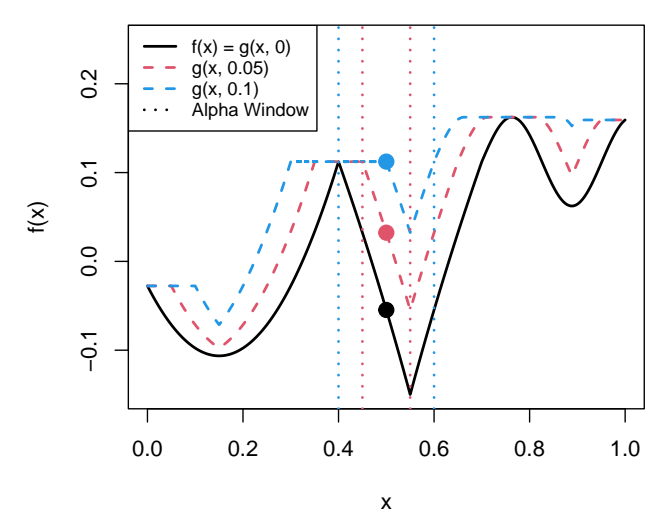


Figure 1: Surface for a 1d multimodal function shown with different adversary levels.

Our goal in this paper is to extend BO via GPs and EI to a richer, more challenging class of optimization problems. In situations where there are a multitude of competing, roughly equivalent local solutions to Eq. (1) a practitioner may naturally express a preference ones which enjoy a wider domain of attraction; i.e., those whose troughs are larger. For example, consider f(x) defined in Eq. (11), provided later in Section 4.2, as characterized by the black line in Figure 1. It has three local minima. The one around x = 0.9 is significantly higher than the other two, and the one around 0.55 has a narrow domain of attraction but lower objective value compared to the one around 0.15. These features mean the robust minimum is the local minimum around x = 0.15. Although BO via GPs/EI would likely explore both domains of attraction to a certain extent eventually, it will in the near term (i.e., for smaller simulation budgets) focus on the deeper/narrower one, providing lower resolution on the solution than many practitioners prefer.

Finding/exploring the robust global solution space requires a modification to both the problem and the BO strategy. Here we borrow a framework first introduced in the math programming literature on robust optimization (e.g., Menickelly and Wild, 2020): an adversary. Adversarial reasoning is popular in the wider reinforcement learning literature (Huang et al., 2011). To our knowledge the mathematical programming notion of an adversary has never been deployed for BO, where it is perhaps best intuited as a form of penalty on "sharp" local minima. Specifically, let x^{α} denote the α -neighborhood of an input x. There are many ways to make this precise depending on context. If x is one-dimensional, then $x^{\alpha} = [x - \alpha, x + \alpha] \equiv [x \pm \alpha]$ is sensible. In higher dimension, one can generalize to an α -ball or hyper-rectangle. More specifics will come later. Relative to that α -neighborhood, an adversary $g(x, \alpha)$ and robust minimum x^r may be defined as follows:

Let
$$g(x,\alpha) = \max_{x \in x^{\alpha}} f(x)$$
 so that $x^r = \underset{x \in [0,1]^d}{\operatorname{argmin}} g(x,\alpha).$ (2)

Figure 1 provides some examples for the f introduced earlier. Observe that the larger α is, the more "flattened" $g(x,\alpha)$ is compared to f(x). In particular, note how the penalization is more severe in the sharper minimum compared to the shallow trough which is only slightly higher than the original, unpenalized function.

The conventional, local, approach to finding the robust solution x^r is best understood as an embellishment of other, conventional, local schemes inspired by Newton's method (e.g., Cheney and Goldstein, 1959). First, extract derivative (and adversarial) information nearby through finite differencing and evaluation at the boundary of x^{α} ; then take small steps that descend the (adversarial) surface. Such schemes offer tidy local convergence guarantees but are profligate with evaluations. When f is expensive, this approach is infeasible. We believe that idea of building an adversary can be ported to the BO framework, making better use of limited simulation resources toward global optimization while still favoring wider domains of attraction.

The crux of our idea is as follows. A GP \hat{f}_n , that would typically be fit to a collection of n evaluations of f in a BO framework, can be used to define the adversarial realization of those same values following the fitted analog of g: $\hat{g}(x_i, \alpha) = \max_{x \in x_i^{\alpha}} \hat{f}(x)$. A second GP \hat{f}_n^{α} can be fit to those $\hat{g}(x_i, \alpha)$ -values, i = 1, ..., N. We call \hat{f}_n^{α} the adversarial surrogate. Then you can use \hat{f}_n^{α} as you would an ordinary surrogate, \hat{f}_n , for example with EI guiding acquisitions. We call this robust expected improvement (REI). There are, of course, myriad details and variations – simplifications and embellishments – that we are glossing over here, and that we shall be more precise about in due course. The most interesting of these may be how we suggest dealing with a practitioner's natural reluctance to commit to a particular choice of α a priori.

Before discussing details, it is worth remarking that the term "robust" has many definitions across the statistical and optimization literature(s). Our use of this term here is more similar to some than others. We do not mean robust to outliers (Martinez-Cantin et al., 2009) as may arise when noisy, leptokurtic simulators f are involved (Beland and Nair, 2017) – though we shall have some thoughts on this setup later. Some refer to robustness as the choice of random initialization of a local optimizer (Taddy et al., 2009). However our emphasis is global. Our definition in Eq. (2), and its BO implementation, bears some similarity to Oliveira et al. (2019) and to so-called "unscented BO" (Nogueira et al., 2016), where robustness over noisy or imprecisely specified *inputs* is considered. However, our adversary entertains a worst-case scenario (e.g., Bogunovic et al., 2018), rather than the stochastic/expected-case. Marzat et al. (2016) also consider worst-case robustness, but focus on so-called "minimax" problems where some dimensions are perfectly controlled ($\alpha = 0$) and others are completely uncontrolled ($\alpha = 1$). Our definition of robustness – x^r in Eq. (2) – emphasizes a worst-case within the α window. Nonetheless, these methods and their test cases make for interesting empirical comparisons, as we demonstrate.

The rest of this paper continues as follows. Section 2 reviews the bare essentials required to understand our proposed methodology. Section 3 introduces our proposed robust BO setup, via adversaries, surrogate modeling and REI, with variations introduced and illustrations along the way. Section 4 showcases empirical results via comparison to those variations and to similar methodology from the recent BO literature. Section 5 then ports that benchmarking framework to a robot pushing problem. Finally, Section 6 concludes with a brief discussion.

2 Review

Here we review the basic elements of BO: GPs and EI.

2.1 Gaussian process regression

A GP may be used to model smooth relationships between inputs and outputs for expensive black-box simulations as follows. Let $x_i \in [0,1]^d$ represent d-dimensional inputs and $y_i = f(x_i)$ be outputs, $i = f(x_i)$

 $1, \ldots, n$. We presume y_i are deterministic realizations of f at x_i , though the GP/BO framework may easily be extended to noisy outputs (see, e.g., Gramacy, 2020, Section 5.2.2 and 7.2.4). Collect inputs into X_n , an $n \times d$ matrix with rows x_i^{\top} , and outputs into column n-vector Y_n . These are the training data $D_n = (X_n, Y_n)$. Then, model as $Y_n \sim \mathcal{N}_n(\mu(X_n), \Sigma(X_n, X_n))$, i.e., presume outputs follow an n-dimensional multivariate normal distribution (MVN).

Often, $\mu(X_n) = 0$ is sufficient for coded inputs and outputs (i.e., after centering and normalization), moving all of the modeling "action" into the covariance structure $\Sigma(\cdot, \cdot)$, which is defined through the choice of a positive-definite, distance-based *kernel*. Here, we prefer a squared exponential kernel, but others such as the Matèrn (Stein, 1999; Abrahamsen, 1997) are common. This choice is not material to our presentation; both specify that the function f, via x_i and y_i , vary smoothly as a function of inverse distance in the input space. Details can be found in Gramacy (2020, Section 5.3.3). Specifically, we fill the covariance structure $\Sigma_{ij} \equiv \Sigma(X_n, X_n)_{ij}$ via

$$\Sigma_{ij} = \tau^2 \left(\exp\left(-\frac{||x_i - x_j||^2}{\theta} \right) + \epsilon \mathbb{I}_{\{i=j\}} \right). \tag{3}$$

The structure in Eq. (3) is hyperparameterized by τ^2 and θ . Let $\hat{\tau}^2$ and $\hat{\theta}$ be estimates for the hyperparameters estimated through the MVN log likelihood. Scale τ^2 captures vertical spread between peaks and valleys f. Lengthscale θ captures how quickly the function changes direction. Larger θ means the correlation decays less quickly leading to flatter functions. Observe that ϵ -jitter (Neal, 1998) is added to the diagonal to ensure numerical stability when decomposing Σ .

Working with MVNs lends a degree of analytic tractability to many statistical operations, in particular for conditioning (e.g., Kalpić and Hlupić, 2011) as required for prediction. Let \mathcal{X} , an $n_p \times d$ matrix, store inputs for "testing." Then, the conditional distribution for $Y(\mathcal{X})$ given $D_n = (X_n, Y_n)$ is also MVN and has a convenient closed form:

$$Y(\mathcal{X}) \mid D_n \sim \mathcal{N}_{n_p}(\mu_n(\mathcal{X}), \Sigma_n(\mathcal{X}))$$
where
$$\mu_n(\mathcal{X}) = \Sigma(\mathcal{X}, X_n) \Sigma^{-1}(X_n, X_n) Y_n$$
and
$$\Sigma_n(\mathcal{X}) = \Sigma(\mathcal{X}, \mathcal{X}) - \Sigma(\mathcal{X}, X_n) \Sigma^{-1}(X_n, X_n) \Sigma(X_n, \mathcal{X}),$$

$$(4)$$

where $\Sigma(\cdot,\cdot)$ extends $\Sigma_{ij} \equiv \Sigma(x_i,x_j)$ in Eq. (3) to the rows of \mathcal{X} and between \mathcal{X} and X_n . The diagonal of the $n_p \times n_p$ matrix $\Sigma_n(\mathcal{X})$ provides pointwise predictive variances which may be denoted as $\sigma_n^2(\mathcal{X})$. Later, we shall use $\operatorname{GP}_{\hat{\theta}}(D_n)$ to indicate a fitted GP surrogate \hat{f}_n to data $D_n = (X_n, Y_n)$ emitting predictive equations $(\mu_n(\cdot), \sigma_n^2(\cdot))$ as in Eq. (4), conditioned on estimated hyperparameters $\hat{\theta}_n$. Note that we are streamlining the notation here somewhat and subsuming $\hat{\tau}^2$ into $\hat{\theta}$. For more information on GPs, see (Gramacy, 2020, Chapter 5) or Santner et al. (2018).

2.2 Expected improvement

Bayesian Optimization (BO) seeks a global minimum (1) under a limited experimental budget of N runs. The idea is to proceed sequentially, $n = n_0, \ldots, N$, and in each iteration n make a greedy selection of the next, $n + 1^{\text{st}}$ run, x_{n+1} , based on solving an acquisition function tied to a surrogate fit to data D_n . The initial n_0 -sized design could be space-filling, for example with a Latin hypercube sample (LHS) or maximin design (Dean et al., 2015, Chapter 17) or, as some have argued (Zhang et al., 2020), purely at random. GPs have emerged as the canonical surrogate model. Although there are many acquisition functions in the literature tailored to BO via GPs, expected improvement (EI) is perhaps the most popular. EI may be described as follows.

Let $f_n^{\min} = \min(y_1, \dots, y_n)$ denote the best "best observed value" (BOV) found so far, after the first n acquisitions (n_0 of which are space-filling/random). Then, define the *improvement* at input location x as $I(x) = \max\{0, f_n^{\min} - Y(x)\}$. I(x) is a random variable, inheriting its distribution from $Y(x) \mid D_n$. If Y(x) is Gaussian, as it is under $GP_{\hat{\theta}}(D_n)$ via Eq. (4), then the expectation of I(x) over the distribution of $Y(x) \mid D_n$ has a closed form:

$$\operatorname{EI}_{n}(x) = \mathbb{E}\{I(x)|D_{n}\} = (f_{n}^{\min} - \mu_{n}(x))\Phi\left(\frac{f_{n}^{\min} - \mu_{n}(x)}{\sigma_{n}(x)}\right) + \sigma_{n}(x)\phi\left(\frac{f_{n}^{\min} - \mu_{n}(x)}{\sigma_{n}(x)}\right),\tag{5}$$

where Φ and ϕ are the standard Gaussian CDF and PDF, respectively. Notice how EI is a weighted combination of mean $\mu_n(x)$ and uncertainty $\sigma_n(x)$, trading off "exploitation and exploration." The first term of the sum is high when $\hat{f}(x)$ is much lower than f_n^{\min} , while the second term is high when the GP has high uncertainty at x.

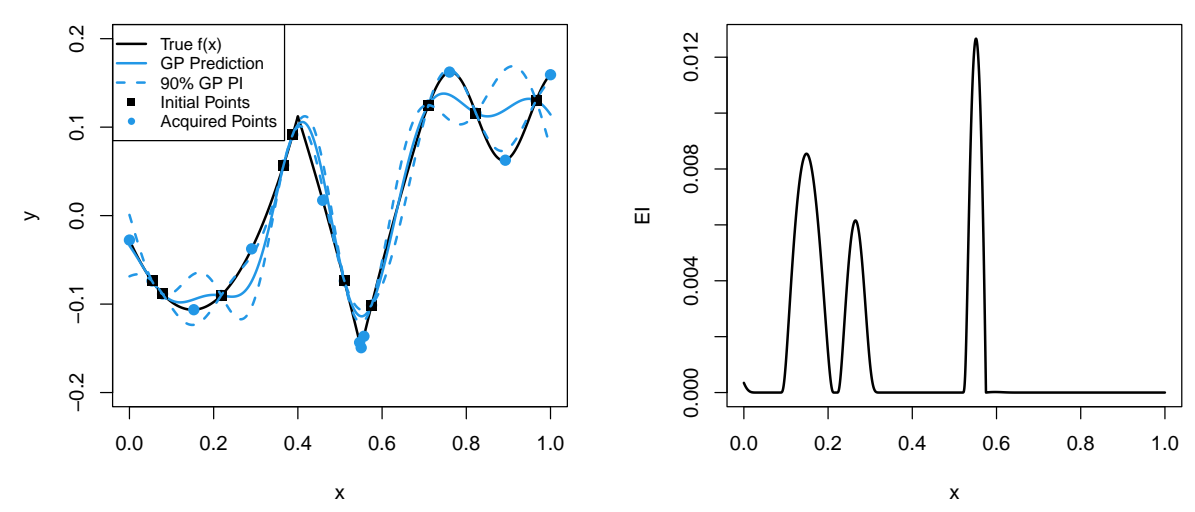


Figure 2: Left: EI-based (EGO) acquisition with $n_0 = 10$ initial points as black squares and 10 acquisitions as blue circles using EGO on the 1D example function from Eq. (11) with initial GP fit in blue. Right: EI using the initial design at different locations of x.

The right panel of Figure 2 shows an EI surface implied by the GP surrogate (blue) shown in the left panel. This fit is derived from n = 10 training data points (black squares) sampled from our f(x) from Figure 1. We will discuss the blue circles momentarily. Observe how EI is high in the two local troughs of minima, near x = 0.15 and x = 0.55, but away from the training data. The total volume (area under the curve) of EI is larger around the left, shallower trough, but the maximal EI location is in the right, spiky trough. This (x near 0.55) is where EI recommends choosing the next, $n + 1^{\text{st}}$ acquisition.

Operationalizing that process, i.e., numerically solving for the next acquisition involves its own, "inner" optimization: $x_{n+1} = \operatorname{argmax}_{x \in [0,1]^d} \operatorname{EI}_n(x)$. This can be challenging because EI is multi-modal. Observe that while f only has two local minima, EI as shown for n = 10 in Figure 2, has three local maxima. So in some sense the inner optimization is harder than the "outer" one. As n grows, the number of local EI maxima can grow. A numerical optimizer such as BFGS (Byrd et al., 1995) is easily stuck, necessitating a multi-start scheme (Burden and Faires, 1989). Another common approach is to use a discrete space-filling set of candidates, replacing a continuous search for $x \in [0,1]^d$ into a discrete one for $x \in \mathcal{X}_{cand}$. Hybrid and smart-candidate schemes are also popular (Scott et al., 2011; Gramacy et al., 2022). In general, we can afford a comprehensive effort toward solving the "inner" optimization because the objective, derived

from $GP_{\hat{\theta}}(D_n)$, is cheap – especially compared to the black-box $f(\cdot)$. Repeated application of EI toward selecting x_{n+1} is known as the *efficient global optimization* algorithm (EGO, Jones et al., 1998).

The blue circles in Figure 2 indicate how nine further acquisitions (ten total) play out, i.e., $10 = n_0, \ldots, n, \ldots, N = 20$ in EGO. Notice that the resulting training data set D_N , combining both black and blue points concentrates acquisitions in the "tip" of the spiky, right trough. The rest of the space, including the shallower left trough, is more uniformly (and sparsely) sampled. Our goal is to concentrate more acquisition effort in the shallower trough.

3 Proposed methodology

Here we extend the EGO algorithm by incorporating adversarial thinking. The goal is to find x^r from Eq. (2) for some α . We begin by presuming a fixed, known α selected by a practitioner.

3.1 The adversarial surrogate

If $\hat{f}_n(x)$ is a surrogate for f(x), then one may analogously notate $\hat{f}_n^{\alpha}(x)$ as a surrogate for $g(x,\alpha)$, an adversarial surrogate. We envision several ways in which $\hat{f}_n^{\alpha}(x)$ could be defined in terms of $\hat{f}_n(x)$, but not many which are tractable to work with analytically or numerically. For example, suppose $Y^{\alpha}(x) = \max_{x' \in x^{\alpha}} Y(x')$, where $Y(x') \sim \mathcal{N}(\mu_n(x'), \sigma_n^2(x'))$, a random variable whose distribution follows the spirit of Eq. (2), but uses the predictive equations of Eq. (4). The distribution of $Y^{\alpha}(x)$ could be a version of $\hat{f}_n^{\alpha}(x)$, at least notionally. However a closed form remains elusive.

Instead, it is rather easier to define $\hat{f}_n^{\alpha}(x)$ as an ordinary surrogate trained on data derived through adversarial reasoning on the original surrogate $\hat{f}_n(x)$. Let Y_n^{α} denote these *adversarial responses*, where each y_i^{α} , for i = 1, ..., n, follows

$$y_i^{\alpha} = \max_{x \in x_i^{\alpha}} \mu_n(x)$$
 where x_i^{α} is the α -neighborhood of the i^{th} entry of X_n , as usual. (6)

There are many sensible choices for how to find y_i^{α} numerically in practice. Newton-based optimizers, e.g., BFGS (Byrd et al., 1995), could leverage closed form derivatives for $\mu_n(x)$, or utilize finite differencing. A simpler option that works well is to instead take $y_i^{\alpha} = \max_{x \in x_i^{\mathcal{B}_{\alpha}(x)}} \mu_n(x)$, where $\mathcal{B}_{\alpha}(x)$ is the discrete set of points on the corners of a box with sides of length α emanating from x. Details for our own implementation are deferred to Section 4.1.

Given Y_n^{α} , an adversarial surrogate may be built by modeling adversarial data $D_n^{\alpha} = (X_n, Y_n^{\alpha})$, i.e., the adversarial responses paired with their original inputs, as a GP. Let $\hat{\theta}_{\alpha}$ denote hyperparameter estimates for GP surrogate $\hat{f}_n^{\alpha}(x)$. Fill in the covariance matrix following Eq. (3), $\Sigma^{\alpha}(\cdot, \cdot)$. Finally, define the adversarial surrogate as

$$\hat{f}_n^{\alpha}(x) \equiv \mathrm{GP}_{\hat{\theta}_{\alpha}}(D_n^{\alpha}) \to (\mu_n^{\alpha}(\cdot), \sigma_n^{2\alpha}(\cdot)) \tag{7}$$

via novel hyperparameter estimates $\hat{\theta}_{\alpha}$ using Y_n^{α} rather than Y_n with predictive equations akin to (4). Since the Y_n^{α} are the original surrogate's (\hat{f}_n) estimate of adversarial response values according f_{α} , \hat{f}_n^{α} may serve as a surrogate for $g(x,\alpha)$ from the left half of Eq. (2).

As a valid GP, \hat{f}_n^{α} can be used in any way another surrogate might be deployed downstream. For example, \hat{f}_n^{α} may be used to acquire new runs via EI, but hold that thought for a moment. To illustrate \hat{f}_n^{α} , the left panel of Figure 3 augments the analogous panel in Figure 2 to include a visual of \hat{f}_n^{α} via μ_n^{α} and error-bars $\mu_n^{\alpha} \pm \sigma_n^{\alpha}$. Perhaps the most notable takeaway from this graph is that the new, red lines, are much higher near the sharp minimum (near x = 0.5), but less dramatically elevated for the wider, dull trough near x = 0.2.

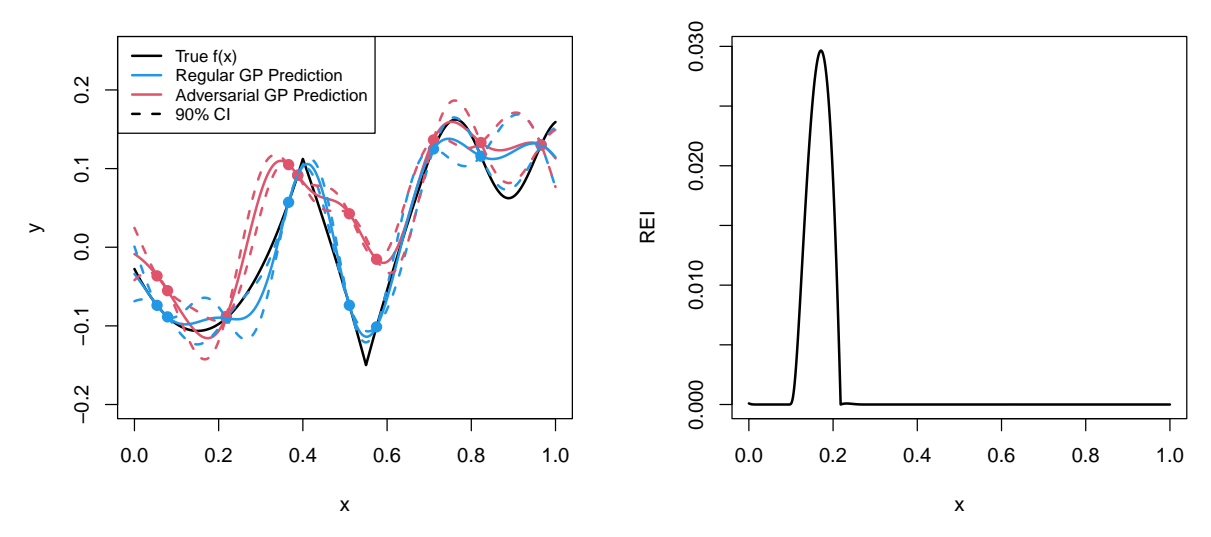


Figure 3: Left: The same black and blue lines from Figure 2. In red, Y_n^{α} are shown as the points with $\hat{f}_n^{\alpha}(x)$ as the curve. Right: Robust expected improvement for the current design.

Also observe in Figure 3 that, whereas for the most part $\mu_n(x) \leq \mu_n^{\alpha}(x)$, this reverses for a small portion of the input domain near x=0.2. That would never happen when comparing f(x) to $g(x,\alpha)$ via Eq. (2). This happens for our surrogates – original \hat{f}_n and adversarial \hat{f}_n^{α} – for two reasons. One is that both are stationary processes because their covariance structure (3) uses only relative distances, resulting in a compromise surface between sharp and dull. Although this is clearly a mismatch to our data-generating mechanism, we have not found any downsides in our empirical work. The possibility of improved performance for non-stationary surrogates is entertained in Section 6. The other reason is that the adversarial data Y_n^{α} , whether via a stationary or (speculatively) a non-stationary surrogate \hat{f}_n , provide a low-resolution view of the true adversary $g(x,\alpha)$ when n is small. Consequently, \hat{f}_n^{α} is a crude approximation to $g(x,\alpha)$, but that will improve with more acquisitions (larger n). What is most important is the EI surface(s) that the surrogate(s) imply. These are shown in the right panel of Figure 3, and discussed next.

3.2 Robust expected improvement

Robust expected improvement (REI), $\text{EI}_n^{\alpha}(\cdot)$, is the analog of in Eq. (5) except using $(\mu_n^{\alpha}(\cdot), \sigma_n^{2\alpha}(\cdot))$, towards solving the mathematical program given in the right half of Eq. (2). Let $f_n^{\alpha,\min} = \min(y_1^{\alpha}, \dots, y_n^{\alpha})$ denote the best estimated adversarial response (BEAR). Then, let

$$\operatorname{EI}_{n}^{\alpha}(x) = \mathbb{E}\{I(x) \mid D_{n}^{\alpha}\} = (f_{n}^{\alpha,\min} - \mu_{n}^{\alpha}(x))\Phi\left(\frac{f_{n}^{\alpha,\min} - \mu_{n}^{\alpha}(x)}{\sigma_{n}^{\alpha}(x)}\right) + \sigma_{n}^{\alpha}(x)\phi\left(\frac{f_{n}^{\alpha,\min} - \mu_{n}^{\alpha}(x)}{\sigma_{n}^{\alpha}(x)}\right). \tag{8}$$

The right panel of Figure 3 shows the REI surface for the same initial setup as Figure 2. We see only one peak, located at the shallower, wider trough compared to three peaks in the EI surface [Figure 2]. Generally speaking, REI surfaces have fewer local maxima compared to EI surfaces because $\hat{f}_n^{\alpha}(x)$ smooths over the peaked regions. Thus the inner optimization of REI often has fewer local minima, generally requiring fewer multi-starts.

Algorithm 1: Robust Expected Improvement

```
input D_n = (X_n, Y_n), x, and \alpha
\hat{f}_n(x) = \operatorname{GP}_{\hat{\theta}}(D_n) \qquad // \text{ with predictive moments in Eq. (4)}
for i = 1, \ldots, n do
\downarrow y_i^{\alpha} = \operatorname{argmax}_{x' \in x_i^{\alpha}} \mu_n(x') \qquad // \text{ adversarial responses, (6)}
D_n^{\alpha} = (X_n, Y_n^{\alpha}) = (X_n, \{y_i^{\alpha}\}_{i=1}^n)
\hat{f}_n^{\alpha}(x) = \operatorname{GP}_{\hat{\theta}_{\alpha}}(D_n^{\alpha}) \qquad // \text{ the adversarial surrogate, (7)}
\operatorname{return} \left(\operatorname{EI}_n^{\alpha}(x)\right) \qquad // \text{ EI using } \hat{f}_n^{\alpha}(x) \text{ from the previous line, (8)}
```

REI is summarized succinctly in Eq. (8) above, but it is important to appreciate that it is a result of a multi-step process. Alg. 1 provides the details: fit an ordinary surrogate, which is used to create adversarial data, in turn defining the adversarial surrogate upon which EI is evaluated. The algorithm is specified for a particular reference location x, used toward solving $x_{n+1} = \operatorname{argmax}_{x \in [0,1]^d} \operatorname{EI}_n^{\alpha}(x)$. It may be applied identically for any x. In a numerical solver it may be advantageous to cache quantities unchanged in x.

With repeated acquisition via EI, over $n=n_0,\ldots,N-1$ being known as EGO, we dub robust efficient global optimization (REGO) as the repeated application of REI towards finding a robust minimum. REGO involves a loop over Alg. 1, with updates $D_n \to D_{n+1}$ after each acquisition. The final data set, $D_N = (X_N, Y_N)$ provides insight into both f(x) and $g(x, \alpha)$ and their minima. Whereas EGO would report BOV f_N^{\min} , and/or the corresponding element x_{bov}^{\star} of X_N , REGO would report the BEAR $f_N^{\alpha,\min}$, the same quantity used to define REI in Eq. (8), and/or input x_{bear}^{\star} .

Post hoc adversarial surrogate

To quantify the advantages of REI/REGO over EI/EGO in our empirical work of Sections 4–5, we consider a post hoc adversarial surrogate. This is the surrogate constructed after running all acquisitions, n_0+1,\ldots,N via EI/EGO, then at N fitting an adversarial surrogate Eq. (7), and extracting the BEAR $f_N^{\alpha,\min}$ rather than the BOV. In other words, the last step is faithful to the adversarial goal, whereas active learning aspects ignore it and proceed as usual. Whereas the BOV from EGO can be a poor approximation to the robust optimum $f(x^r)$ of Eq. (2), the BEAR from a post hoc adversarial surrogate can potentially be better. Comparing two BEAR solutions, one from REGO and one from a post hoc EGO surrogate, allows us to separately explore the value of REI acquisitions from post hoc adversarial surrogates, \hat{f}_N^{α} .

To illustrate on our running example, consider the outcome of EGO, from the left panel of Figure 2, recreated in the left panel of Figure 4. In both, the union of black and blue points comprise D_N . In Figure 4 the dashed blue curve provides the post hoc adversarial surrogate, \hat{f}_N^{α} , from these runs, with the BOV and BEAR indicated as magenta diamonds and triangles, respectively. Notice that for EGO, the BOV is around the global, peaked minimum, but the BEAR captures the shallow, robust minimum. The analogous REGO run, via EI acquisitions (red circles) and adversarial surrogate (red lines) is shown in the right panel of Figure 4. Here BEAR and BOV estimates are identical since REGO does not explore the peaked minimum.

Looking at both panels of Figure 4, the BEAR offers a robust solution for both EGO or REGO. However, EGO puts only one of its acquisitions in the wide trough compared to four from REGO. Consequently, REGO's BEAR offers a more accurate estimate for x^r . With only N=20 points in 1d, any sensible acquisition strategy should yield a decent meta-model for f(x) and $g(x,\alpha)$, so we may have reached the limits of the utility of this illustrative example. In Sections 4–5 we intend to provide more compelling

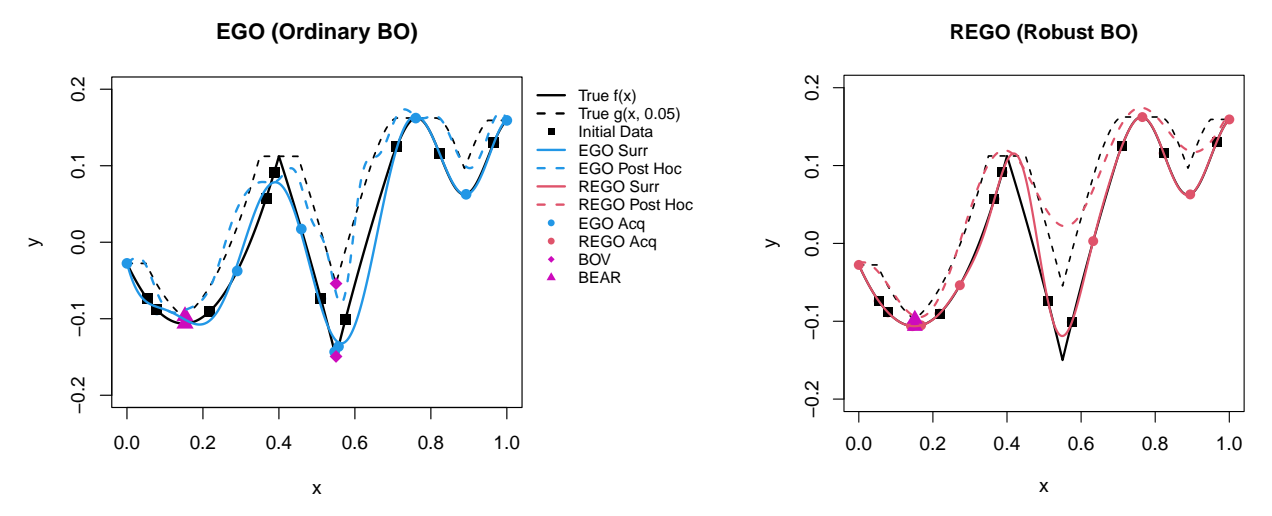


Figure 4: Left: Surrogate and post hoc surrogate fits after EGO acquisitions (N = 20 and $n_0 = 10$) on Eq. (11). Right: Same except REGO where BOV and BEAR are the same.

evidence that REGO is better at targeting robust minima. Before turning to that empirical study, we introduce two REI variations that feature in some of those examples.

Unknown and vector-valued α

Until this point we have presumed fixed, scalar α , perhaps specified by a practitioner. In the case of inputs x coded to the unit cube $[0,1]^d$, a choice of $\alpha=0.05$, say, represents a robustness specification of 5% in each coordinate direction (totaling 10% of each dimension), i.e., where $x^{\alpha} \equiv [x_j \pm \alpha : j = 1, \ldots, d]$. This intuitive relationship can be helpful in choosing α , however one may naturally wish to be "robust" to this specification. Suppose instead we had an α_{\max} in mind, where $0 \le \alpha \le \alpha_{\max}$. One option is to simply run REGO with $\alpha \leftarrow \alpha_{\max}$, i.e., basing all REI acquisitions on α_{\max} instead. Although we do not show this to save space, performance (via BEAR) of α_{\max} relative to a nominal α rapidly deteriorates as the gap between α_{\max} and α widens.

A better method is to base REI acquisitions on all α -values between zero and α_{\max} by integrating over them: $\overline{\mathrm{EI}}_n^{\alpha_{\max}} = \int_0^{\alpha_{\max}} \mathrm{EI}_n^{\alpha}(x) \ dF(\alpha)$, say over uniform measure F. We are not aware of an analytically tractable solution, in part because embedded in $\mathrm{EI}_n^{\alpha}(x)$ are complicated processes such as determining adversarial data, and surrogates fit thereupon. But quadrature is relatively straightforward, either via Monte Carlo (MC) $\alpha^{(t)} \sim F$, for $t = 1, \ldots, T$, over a grid $\{0 = \alpha^{(1)}, \ldots, \alpha^{(T)} = \alpha_{\max}\}$. Define

$$\overline{\mathrm{EI}}_{n}^{\alpha_{\mathrm{max}}} \approx \frac{1}{T} \sum_{t=1}^{T} \mathrm{EI}_{n}^{\alpha^{(t)}}(x) \quad \text{ for the former,} \quad \text{or} \quad \overline{\mathrm{EI}}_{n}^{\alpha_{\mathrm{max}}} \approx \frac{1}{T} \sum_{t=1}^{T} \mathrm{EI}_{n}^{\alpha^{(t)}}(x) F(\alpha^{(t)}), \tag{9}$$

for the latter. Both may be implemented by looping over Alg. 1 with different $\alpha^{(t)}$ values, and then averaging to take $x_{n+1} = \operatorname{argmax}_{x \in [0,1]^d} \overline{\mathrm{EI}}_n^{\alpha_{\max}}$. Both approximations improve for larger T.

With random $\alpha^{(t)} \sim F$, even a single draw (T=1) suffices as an unbiased estimator – though clearly with high variance. This has the advantage of a simpler implementation, and faster execution as no loop over Alg. 1 is required. In our empirical work to follow, we refer to this simpler option as the "rand" approximation, and the others (MC or grid-based) as "sum". It is remarkable how similarly these options perform, relative to one another and to a nominal REI with a fixed α -value. One could impose $\alpha_{\min} > 0$ similarly, though we do not entertain this variation here.

As a somewhat orthogonal consideration, it may be desirable to entertain different levels of robustness – different α -values $\{\alpha_1, \ldots, \alpha_d\}$ – in each of the d coordinate directions. The only change this imparts on the description above is that now $x^{\alpha} = [x_j \pm \alpha_j : j = 1, \ldots, d]$, a hyperrectangle rather than hypercube. Other quantities such as $g(x, \alpha)$ and $\text{EI}_n^{\alpha}(x)$ remain as defined earlier with the understanding of a vectorized $\alpha = \{\alpha_1, \ldots, \alpha_d\}$ under the hood. Using vectorized α_{max} in Eq. (9) requires draws from a multivariate F, which may still be uniform, or a higher dimensional grid of $\alpha^{(t)}$, recognizing that we are now approximating a higher dimensional integral.

4 Implementation and benchmarking

Here we provide a description of our implementation, variations, methods of our main competitors, evaluation metrics and ultimately provide a suite of empirical comparisons.

4.1 Implementation details

Our main methods (REI/REGO, variations and special cases) are coded in R (R Core Team, 2021). These codes may be found, alongside those of our comparators and all empirical work in this paper, in our public Git repository: https://bitbucket.org/gramacylab/ropt/. GP surrogate modeling for our new methods – our competitors may leverage different subroutines/libraries – is provided by the laGP package (Gramacy, 2016), on CRAN. Those subroutines, which are primarily implemented in C, leverage squared exponential covariance structure (3), and provide analytic $\hat{\tau}^2$ conditional on lengthscale θ . In our experiments, θ is fixed to appropriate values in order to control MC variation that otherwise arises in repeated MLE-updating of $\hat{\theta}$, especially in small-n cases. More details are provided as we introduce our test cases, with further discussion in Section 6. Throughout we use $\epsilon = 10^{-8}$ in Eq. (3), as appropriate for deterministic blackbox objective function evaluations. For ordinary EI calculations we use add-on code provided by Gramacy (2020, Chapter 7.2.2). All empirical work was conducted on an 8-core hyperthreaded Intel i9-9900K CPU at 3.60 GHz with Intel MKL linear algebra subroutines.

Section 3.1 introduced several possibilities for solving y_i^{α} , whose definition is provided in Eq. (6). Although numerical optimization, e.g. BFGS, is a gold standard, in most cases we found this to be overkill, resulting in high runtimes for all $(N-N_0)$ acquisitions with no real improvements in accuracy over the following, far simpler alternative. We prefer quickly optimizing over the discrete set $x^{\mathcal{B}_{\alpha}(x)}$ comprising of a box extending α -units out in each coordinate direction from x, or its vectorized analog as described in Section 3.2. This "cornering" alternative occasionally yields $y_i^{\alpha} < y_i$, which is undesirable, but this is easily mitigated by augmenting the box $x^{\mathcal{B}_{\alpha}(x)}$ to contain a small number of intermediate, grid locations in each coordinate direction. Using an odd number of such intermediate points ensures $y_i^{\alpha} \ge y_i$. We use three additional grid points per input in our higher-dimensional exercises, and none in lower dimensional ones. We find that a d-dimensional grid formed from the outer product for each coordinate (i.e., a $2^5 = 32$ -point-grid for d = 2) facilitates a nice compromise between computational thrift, and accuracy of adversarial y_i^{α} -values compared to the cumbersome BFGS-based alternative.

In our test problems, which are introduced momentarily and utilize inputs coded to $[0,1]^d$, we compare each of the three variations of REGO described in Section 3. These comprise: (1) REI with known α (Alg. 1); (2) novel $\alpha \sim \text{Unif}(0, \alpha_{\text{max}})$ at acquisition; and (3) averaging over a sequence of $\alpha \in [0, \alpha_{\text{max}}]$ (9). For all examples, we set $\alpha_{\text{max}} = 0.2$ and average over five equally spaced values. In figures, these methods are denoted as "known", "rand" and "sum", respectively. After each acquisition, we use the post hoc adversarial surrogate to find the BEAR operating conditions: x_{bear}^* and $f_N^{\alpha, \text{min}}$ in order to track progress.

As representatives from the standard BO literature, we compare against the following "strawmen":

EGO (Jones et al., 1998), where acquisitions are based on EI (5; and "EY" (Gramacy, 2020) which works similarly to EGO, except acquisitions are selected minimizing $\mathbb{E}[Y(x) \mid D_N]$: $x_{\text{new}}^{\text{EY}} = \operatorname{argmin}_{x \in [0,1]^d} \mu_n(x)$. In other words, EY acquires the point that the surrogate predicts has the lowest mean. Since it does not incorporate uncertainty $(\sigma_n(x))$, repeated EY acquisition often stagnates in one region – usually a local minima – rather than exploring new areas like EI does. In our figures, these comparators are indicated, as follows: "ego", and "ey" respectively for EGO and EY with progress measured by BOV: x_{bov}^* and f_N^{min} . Finally, we consider the post hoc adversary with progress measured by BEAR for EGO ("egoph") and uniform random sampling ("unif"). In the figures, REI methods are solid curves with robust competitors dashed and regular BO dotted.

Our final comparator is StableOPT from Bogunovic et al. (2018). For completeness, we offer the following by way of a high-level overview; details are left to their paper. Bogunovic et al. assume a fixed, known α , although we see no reason why our extensions for unknown α could not be adapted to their method as well. Their algorithm relies on confidence bounds to narrow in on x^r . Let $\mathrm{ucb}_n(x) = \mu_n(x) + 2\sigma_n(x)$ denote the upper 95% confidence bound at x for a fitted surrogate \hat{f}_n , and similarly $\mathrm{lcb}_n(x) = \mu_n(x) - 2\sigma_n(x)$ for the analagous lower bound. Then we may translate their algorithm into our notation, shown in Alg. 2, furnishing the n^{th} acquisition. Similar to REGO, this may then be wrapped in a loop for multiple acquisitions. We could not find any public software for StableOPT, but it was relatively easy to implement in R; see our public Git repo.

Algorithm 2: StableOPT

```
\begin{array}{ll} \text{input } D_{n-1} = (X_{n-1}, Y_{n-1}) \text{ and } \alpha \\ \hat{f}_{n-1}(x) = \operatorname{GP}_{\hat{\theta}}(D_{n-1}) & \text{// with predictive moments in Eq. (4)} \\ \tilde{x}_n = \operatorname{argmin}_{x \in [0,1]^d} \max_{a \in [-\alpha,\alpha]} \operatorname{lcb}_{n-1}(x+a) & \text{// where we think } x^r \text{ is} \\ a_n = \operatorname{argmax}_{a \in [-\alpha,\alpha]} \operatorname{ucb}_{n-1}(\tilde{x}_n+a) & \text{// worst point within } \tilde{x}_n^{\alpha} \\ \text{return } (\tilde{x}_n + a_n, f(\tilde{x}_n + a_n))) & \text{// sample from } f \text{ and return} \end{array}
```

Rather than acquiring new runs nearby likely x^r , StableOPT samples the worst point within \tilde{x}_n^{α} . Consequently, its final X_N does not contain any points thought to be x^r . Bogunovic et al. recommend selecting x_{bear}^* from all \tilde{x}_n rather than the actual points sampled, all $\tilde{x}_n + a_n$, using notation introduced in Alg. 2. We generally think it is a mistake to report an answer at an untried input location. So in our experiments we calculate x_{bear}^* for StableOPT as derived from a final, post hoc adversary calculation [Section 3.2]. In figures, this comparator is denoted as "stable".

The general flow of our benchmarking exercises coming next [Section 4.2] is as follows. Each optimization, say in input dimension d, is seeded with a novel LHS of size $n_0 = 5 + 5d$ that is shared for each comparator. Acquisitions, $n = n_0 + 1, ..., N$, separate for each comparator up to a total budget N (different for each problem), are accumulated and progress is tracked along the way. Then this is repeated, for a total of 1,000 MC repetitions. To simplify notation, let $x_{\rm b,n}^*$ be either $x_{\rm bear}^*$ or $x_{\rm bov}^*$, depending on if using BEAR or BOV, after the $n^{\rm th}$ acquisition. We utilize the following two metrics to compare BEAR or BOV across methods using the true adversary:

$$r(x_{b,n}^*) = g(x_{b,n}^*, \alpha) - g(x^r, \alpha) \qquad d(x_{b,n}^*) = ||x_{b,n}^* - x^r||,$$
(10)

where x^r is the x location of the true robust minimum. The first metric is similar to the concept of regret from decision theory (Blum and Mansour, 2007; Kaelbling et al., 1996) at the suggested $x_{\rm b,n}^*$. Regret measures how much you lose out by running at $x_{\rm b,n}^*$ compared to x^r . Regret is always nonnegative since by definition, $x^r = \operatorname{argmin}_{x \in [0,1]^d} g(x,\alpha)$. The second metric is the distance from $x_{\rm b,n}^*$ to x^r . For both

metrics, lower is better with 0 being the theoretical minimum if a method correctly identifies exactly x^r as the BEAR or BOV.

4.2 Empirical comparisons

One-dimensional examples

The left panel of Figure 5 shows the 1d RKHS function used by Assael et al. (2014), and an adversary with $\alpha = 0.03$. Observe how f has a smooth region for low x values and a wiggly region for high x. With

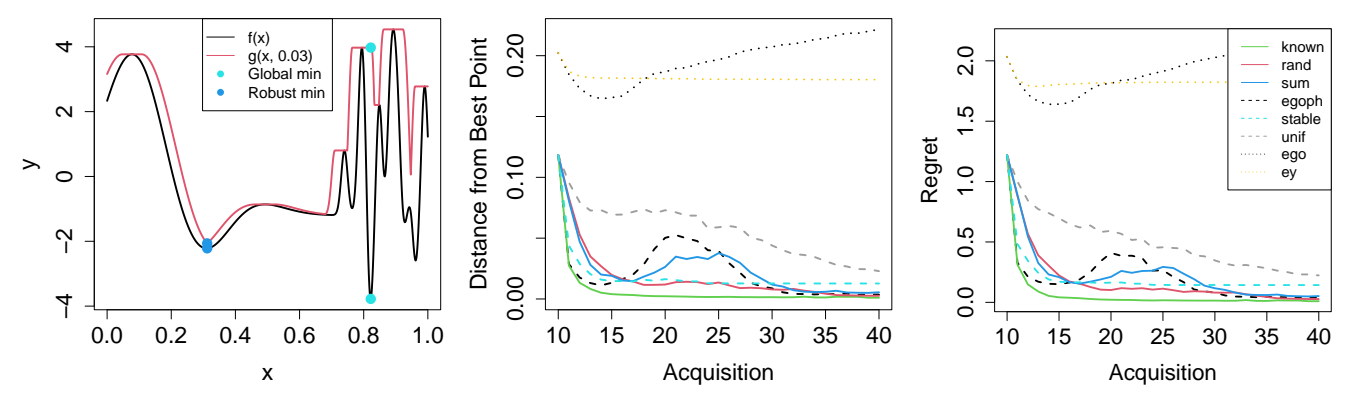


Figure 5: Left: The RKHS function and the robust surface with $\alpha = 0.03$. Middle: $d(x_{\rm b,n}^*)$ after each acquisition. Right: $r(x_{\rm b,n}^*)$ after each acquisition.

 $\alpha=0.03,\,x^r=0.312$ whereas $x^*=0.822$. The adversary is bumped up substantially nearby x^* because the surface is so wiggly there. Here we consider a final budget of N=40 with $\theta=0.01$. Results are provided in the middle and right panels of Figure 5. Observe that REGO with known α performs best as it quickly gets close to x^r , and more-or-less stays there. EGO with post hoc adversary does well at the beginning, but after twenty acquisitions in, it explores around x^* more, retarding progress (explaining the "bump") toward x^r . "Sum"-based REI has a somewhat slighter bump. Averaging over smaller α -values favors exploring the wiggly region. StableOPT caps out at a worse solution than any of the REI-based methods. Those based on BOV, like "ego" and "ey" fare worst of all. Even worse than acquiring "unif" ormly at random.

Figure 6 shows a 1d test function of our own creation, first depicted in Figure 1, defined as:

$$f(x) = \begin{cases} 3.5(x - 0.15)^2 + \log(1.3) & x < 0.4\\ \log(1 + |2(x - 0.55)|) & 0.4 \le x < 0.7\\ \frac{1}{20}\sin(25x - 17.5) + \log(1.3) & 0.7 \le x. \end{cases}$$
(11)

In this problem, $x^* = 0.55$ and $x^r = 0.15$ using $\alpha = 0.075$. All GP surrogates used $\theta = 0.25$. We see a similar story here as for our first test problem. The only notable difference here is that EGO does not get drawn into the peaky region, likely because it is less pronounced. EGO favors sampling around x^* initially, but eventually explores the rest of the input space, including around x^r . Interestingly, REGO with known α performs a little worse than either of the unknown α methods.

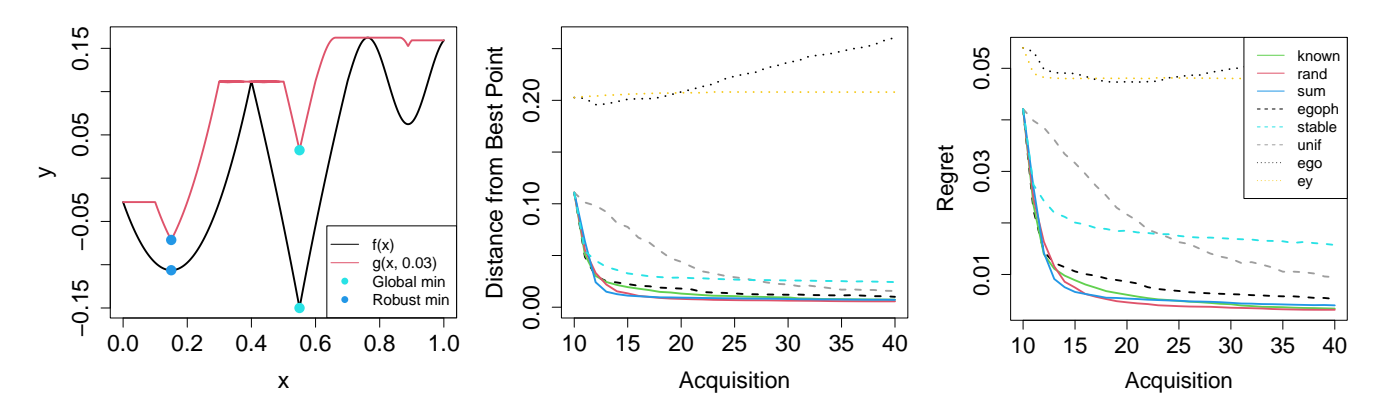


Figure 6: Left: The Figure 1 function and the robust surface with $\alpha=0.075$. Middle: $d(x_{\rm b,n}^*)$ after each acquisition. Right: $r(x_{\rm b,n}^*)$ after each acquisition.

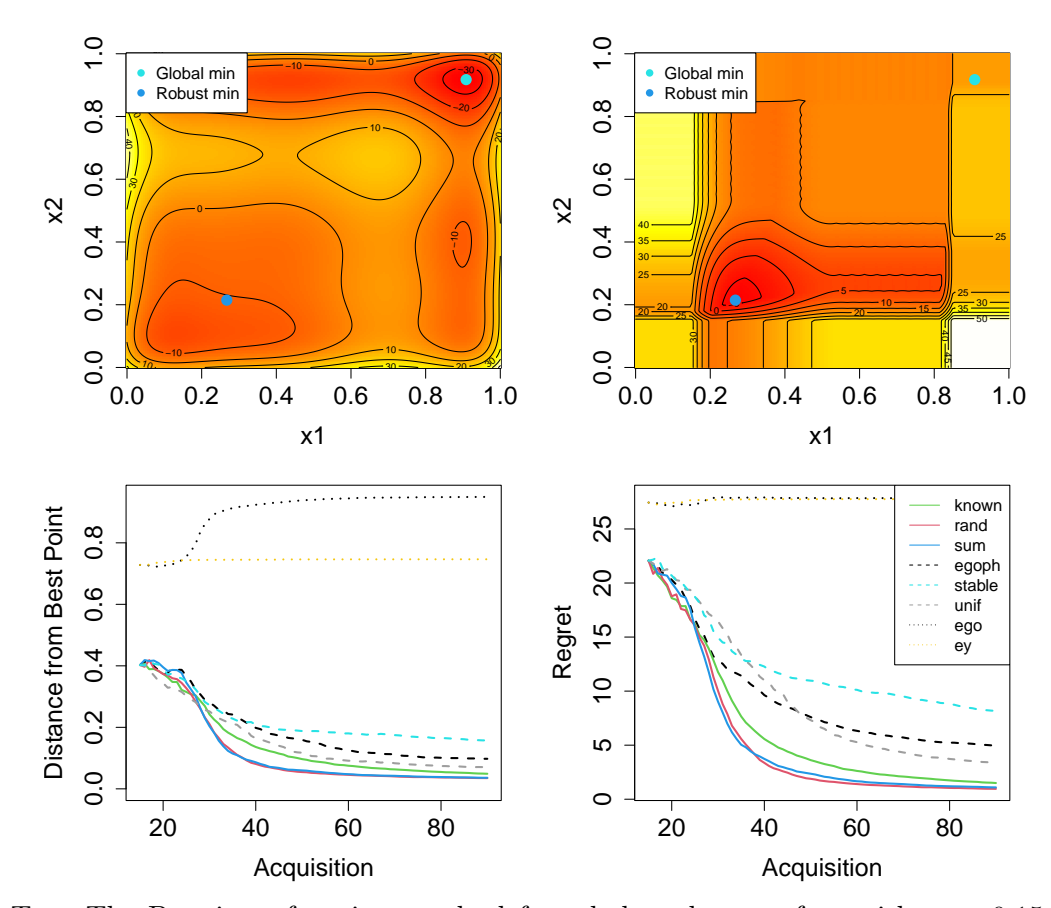


Figure 7: Top: The Bertsimas function on the left and the robust surface with $\alpha = 0.15$ on the right. Bottom: $d(x_{\mathrm{b,n}}^*)$ (left) and $r(x_{\mathrm{b,n}}^*)$ (right) after each acquisition.

Two-dimensional examples

The top-left panel of Figure 7 shows a test problem from Bertsimas et al. (2010), defined as:

$$f(x_1, x_2) = -2x_1^6 + 12.2x_1^5 - 21.2x_1^4 + 6.4x_1^3 + 4.7x_1^2 - 6.2x_1 - x_2^6 + 11x_2^5 - 43.3x_2^4$$

$$+ 74.8x_2^3 - 56.9x_2^2 + 10x_2 + 4.1x_1x_2 + 0.1x_1^2x_2^2 - 0.4x_1x_2^2 - 0.4x_1^2x_2.$$
(12)

We negated this function compared to Bertsimas et al., who were interested in maximization. Originally, it was defined on $x_1 \in [-0.95, 3.2]$ and $x_2 \in [-0.45, 4.4]$ with $x^* = (2.8, 4.0)$. We coded inputs to $[0, 1]^2$ so that the true minimum is at (0.918, 0.908). In the scaled space, $x^r = (0.2673, 0.2146)$ using $\alpha = 0.15$. We used $\theta = 1.1$ and N = 90. The bottom row of panels in Figure 7 show that non-fixed α for REGO can give superior performance in early acquisitions. StableOPT performs worse with this problem because the objective surface near x^r is relatively more peaked, say compared to the 1d RKHS example. Regret is trending toward 0 when using BEAR for acquisitions, with REGO-based methods leading the charge. EGO with post hoc adversary performs much worse for this problem. EGO-based acquisitions heavily cluster near x^* which thwarts consistent identification of x^r even with a post hoc surrogate.

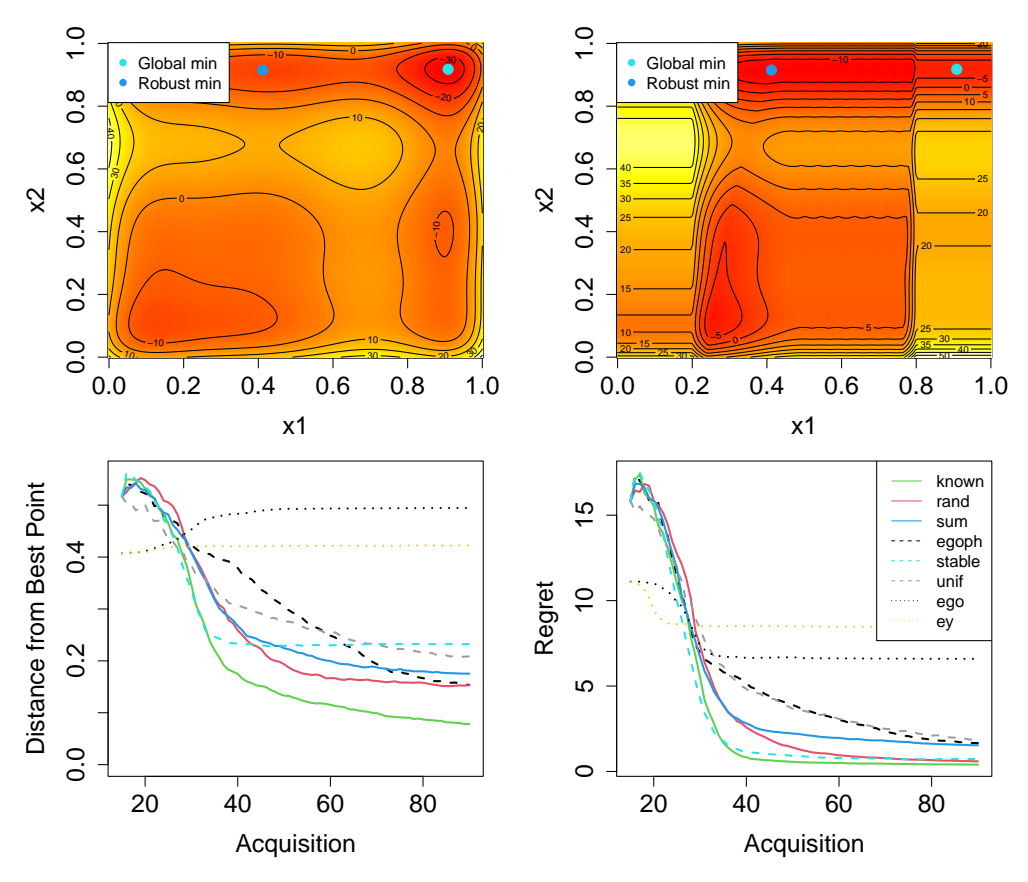


Figure 8: Top: The Bertsimas function on the left with the robust surface with $\alpha = (0.2, 0)$ on the right. Bottom: $d(x_{\text{b,n}}^*)$ (left) and $r(x_{\text{b,n}}^*)$ (right) after each acquisition.

Figure 8 considers the same test problem (12), except this time we use $\alpha = (0.2, 0)$, meaning no robustness required in x_2 . This moves x^r to (0.412, 0.915) in the scaled space. In this problem, the robust surface is fairly flat meaning that when an algorithm finds $x_2 = 0.915$, $x_1 \in [0.35, 0.75]$ gives a similar robust output. For that reason, all of the methods perform worse when trying to pin down the exact x_1 location, so by looking at metric $d(x_b^*)$ from Eq. (10), all methods appear to be doing worse than looking at $r(x_b^*)$ which goes to 0 relatively quickly. A shallower robust minimum favors StableOPT. Since that comparator never actually evaluates at x^r , on this problem it suffices to find $x_1 \in [0.35, 0.75]$, which it does quite easily. Knowing true α for REI helps considerably. This makes sense because omitting an entire dimension from robust consideration is quite informative. Nevertheless, alternatives using random and aggregate α -values perform well.

Higher dimension

Our final set of test functions comes from the Rosenbrock family (Dixon and Szego, 1979),

$$\sum_{i=1}^{d-1} \left(100(x_{i+1} - x_i)^2 + (x_i - 1)^2 \right). \tag{13}$$

defined in arbitrary dimension d. Originally in $[-2.48, 2.48]^d$, we again scale to $[0, 1]^d$. Although our focus here will be on d = 4, visualization easier in 2d. The top-left panel of Figure 9 shows a visual with outputs

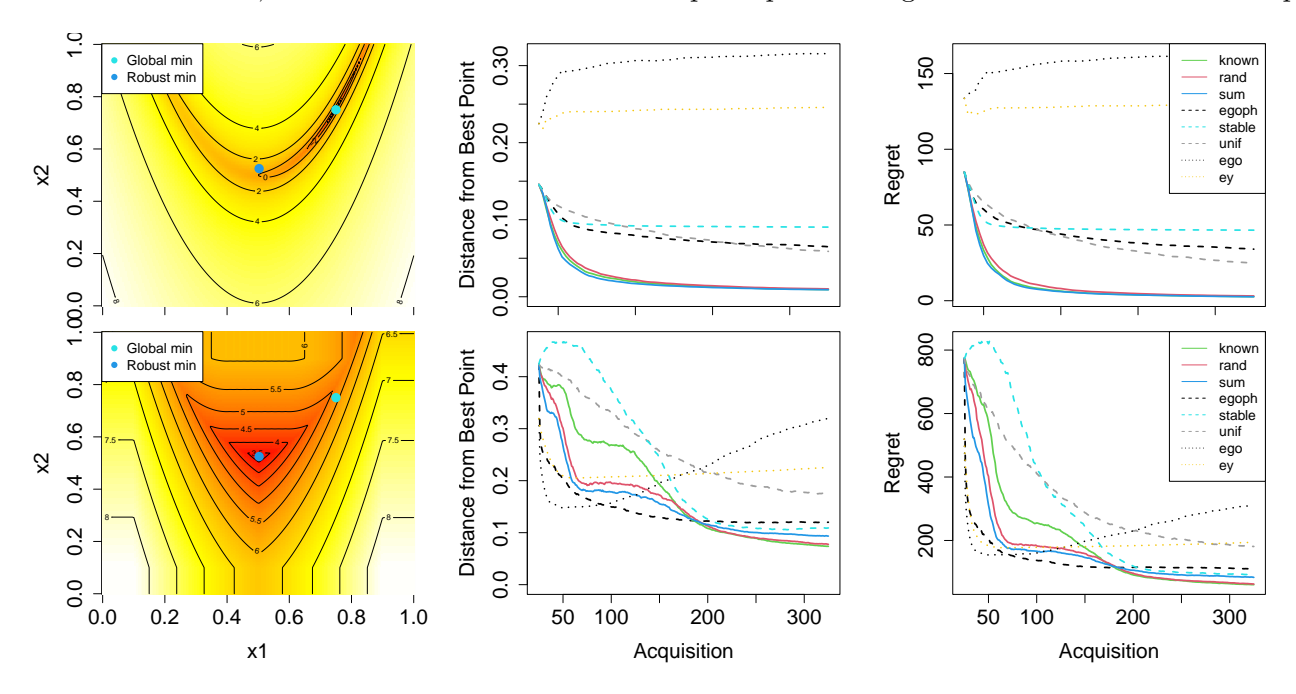


Figure 9: Left: 2d log Rosenbrock function on the top and the robust surface with $\alpha = 0.1$ on the bottom. Top: $d(x_{b,n}^*)$ in the middle and $r(x_{b,n}^*)$ on the right for 2d. Bottom: similarly in 4d.

on the log scale for a 2d case. Here $x^* = (0.75, 0.75)$ and $x^r = (0.503, 0.525)$ when $\alpha = 0.1$. A 2d visual of this adversary is in the bottom-left panel. In 2d, we set $\theta = 0.9$ and in 4d, we use $\theta = 0.05$. Results for 2d are in the top row (middle and right panels), and for 4d are in the bottom row, respectively. REGO shines in both cases because x^* is in a peaked region and x^r is in a shallow one. EGO with post hoc adversary does well early on, but stops improving much after about 150 acquisitions. StableOPT has the same issues of sampling around x^r that we have seen throughout – never actually sampling it.

4.3 Supplementary empirical analysis

An instructive, qualitative way to evaluate each acquisition algorithm is to inspect the final collection of samples (at N), to see visually if things look better for robust variations. Figure 10 shows the final samples of one representative MC iteration for EGO, REGO with random α and StableOPT for 2d Rosenbrock (13) (left panel) and both Bertsimas (12) variations (middle and right panels).

Consider Rosenbrock first. Here, EGO has most of its acquisitions in a mass around x^* with some acquisitions dispersed throughout the rest of the space. This is exactly what EGO is designed to do: target the global minimum, but still explore other areas. REGO has a similar amount of space-fillingness,

but the target cluster is focused on x^r rather than x^* . On the other hand, StableOPT has almost no exploration points. Nearly all of its acquisitions are on the perimeter of a bounding box around x^r . While StableOPT does a great job of picking out where x^r is, intuitively we do not need 70+ acquisitions all right next to each other. Some of those acquisitions could better facilitate learning of the surface by exploring elsewhere.

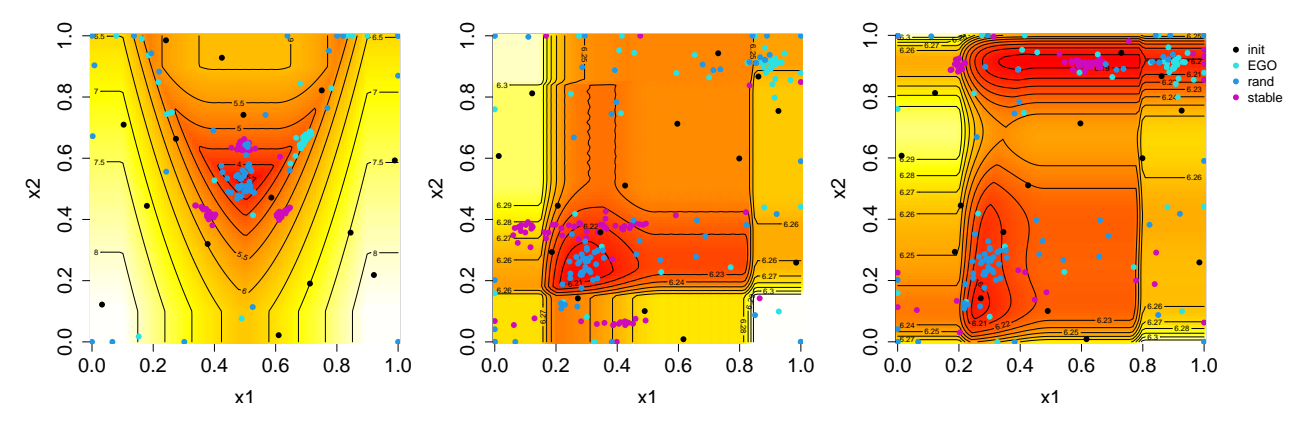


Figure 10: Sample acquisitions for EGO, REGO with random α and StableOPT for 2d Rosenbrock with $\alpha = 0.1$ (left), and Bertsimas functions with $\alpha = 0.15$ (middle), and $\alpha = (0.2, 0)$ (right).

Moving to the Bertsimas panels of the figure, similar behavior may be observed. REGO and EGO have some space-filling points, but mostly target x^r for REGO and x^* for EGO. StableOPT again puts almost all of its acquisitions near x^r with relatively little exploration. But the main takeaway from the Bertsimas plots is that, since REGO does not require setting α beforehand, it gives sensible designs for multiple α values (the blue points are the exactly the same in both panels). Looking more closely at the REGO design, observe that all three minima (global and robust with $\alpha = 0.15$ and $\alpha = (0.2, 0)$) have many acquisitions around them. This shows the power of REGO, capturing all levels of α and allowing the user to delay specifying α until after experimental design.

Timings for each method/problem are in Figure 11. Comparators "egoph" and "ego" report identical timings because they involve the same EI acquisition function. As you might expect, "unif" and EY have the lowest times because they do less work. For the more competitive methods, REGO is generally a little slower than EGO, but often faster than StableOPT. None of these timings are substantial compared to black-box evaluations typically involved in BO enterprises.

5 Robot pushing

Here we consider a real world example to measure the effectiveness of REI. The robot pushing simulator (Kaelbling and Lozano-Perez, 2017, https://github.com/zi-w/Max-value-Entropy-Search) has been used previously to test ordinary BO (Wang et al., 2017; Wang and Jegelka, 2017) and robust (Bogunovic et al., 2018) BO methodology. The simulator models a robot hand, with up to 14 tunable parameters, pushing a box with the goal of minimizing distance to a target location. Following Wang and Jegelka (2017), we consider varying four of the tunable parameters, as detailed in Table 1. This simulator is coded in Python and uses an engine called Box2D (Catto, 2011) to simulate the physics of pushing. Also following Wang and Jegelka (2017), we consider two cases: one with a fixed hand angle, always facing the box, determined to be $r_{\theta} = \arctan(\frac{r_y}{r_x})$; and the other allowing for all 4 parameters to vary. These create 3d and 4d problems that we call "push3" and "push4", respectively

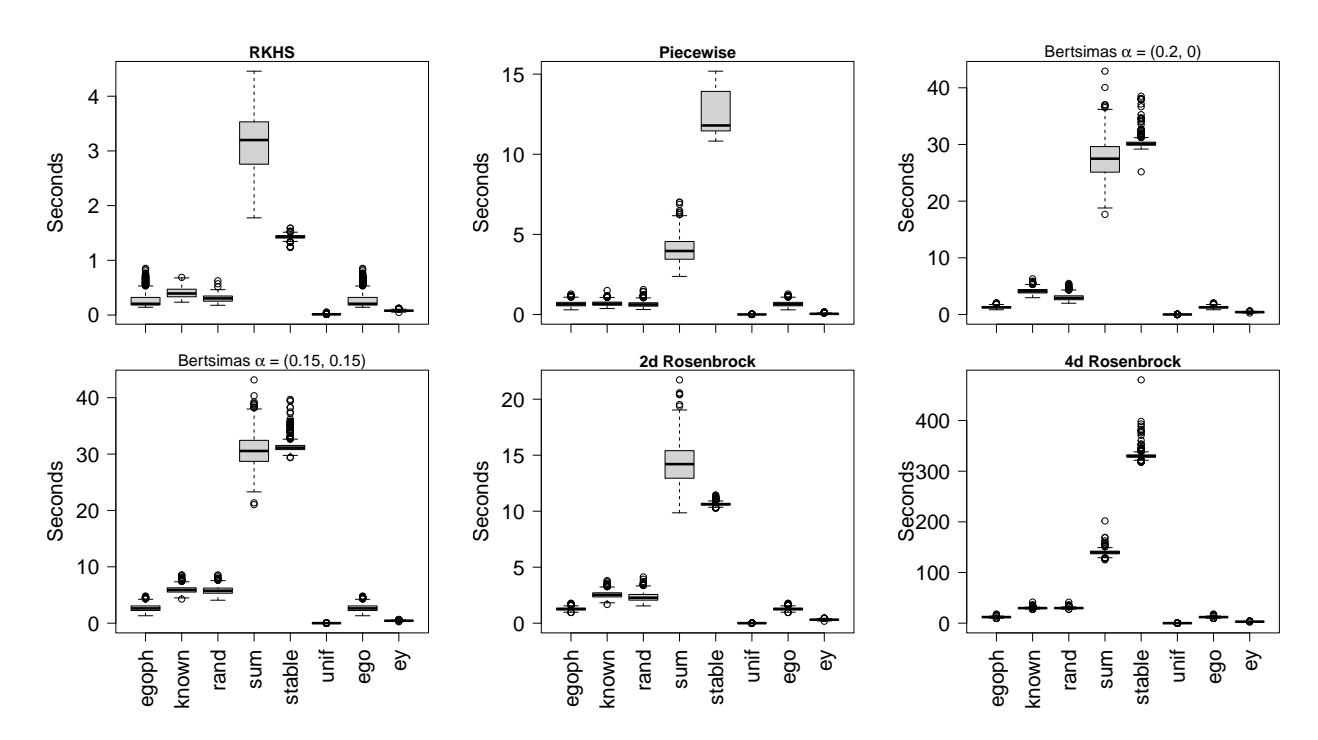


Figure 11: Cumulative timings for each method/test function.

Parameter	Role	Range
r_x	initial x-location	[-5, 5]
r_y	initial y-location	[-5, 5]
$r_{ heta}$	initial angle	$\left[-\frac{\pi}{2},\frac{\pi}{2}\right]$
t_r	pushing strength	[1, 30]

Table 1: Parameters for the robot pushing simulator.

We consider two further adaptations. First, we de-noised the simulator, so that it is deterministic, which is more in line with our previous examples. Second, rather than look at a single target location, we take the minimum distance to two, geographically distinct target locations under squared and un-squared distances respectively. We do this in order to manifest a version of the problem that would require robust analysis. Having the box pushed the full distance toward either target, minimizing the objective, yields an output of 0 since $0^2 = 0$. However, the minimum around the unsquared target will be shallower because the unsquared surface increases slower when the distance to the target is greater than 1. Robust BO prefers exploring the unsquared minimum while an ordinary, non-robust method would show no preference. Similarly, a BOV performance metric is indifferent to the target locations, while BEAR would favor the unsquared target.

For both "push3" and "push4" variations, we somewhat arbitrarily fixed the target locations at (-3,3) and (3,-3) with the latter being the target with squared distance outputs. Since the unsquared location is in the top-left quadrant, the optimal robust location involves starting the robot hand in the bottom-right so that it pushes the box up and left. Furthermore, because the robot cannot perfectly control the initial hand location, if it is close to the origin, a minor change in r_x or r_y leads to the hand pushing away from the target location. For "push3" we use $\alpha = 0.1$, $x^r = (5, -5, 25.4)$, meaning the robot hand starts as far in the bottom-right as possible and pushes quite hard. The true setting $g(x^r, 0.1) = 1.37$ is lower than analogously pushing toward the squared target location, g((-5, 5, 25.4), 0.1) = 1.88, solely due to squaring as $1.37^2 \approx 1.88$.

We compare each of the methods from Section 4.2 in a similar fashion by initializing with an LHS

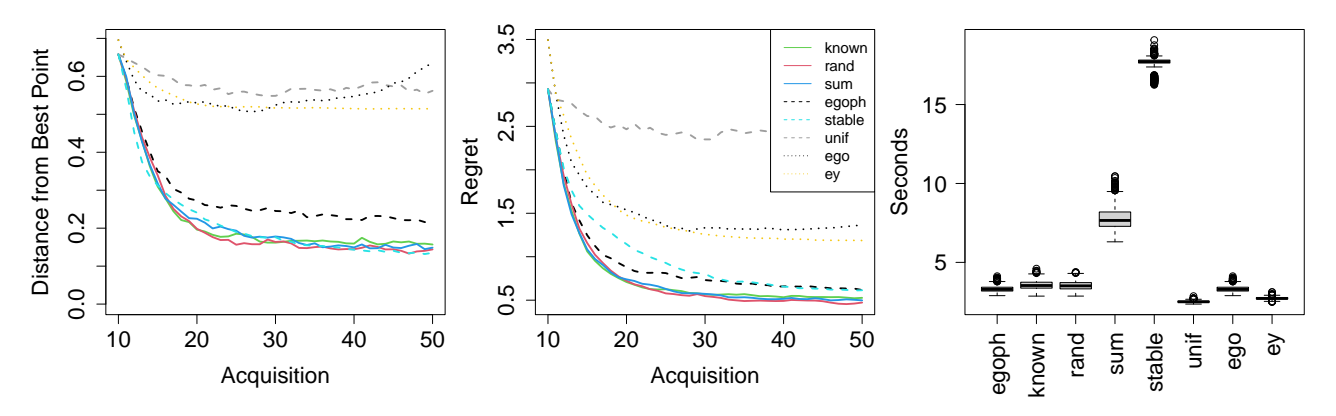


Figure 12: Results for "push3" $\alpha=0.1$: $d(x_{\rm b,n}^*)$ (left), $r(x_{\rm b,n}^*)$ (middle) and cumulative time (right).

of size $n_0 = 10$ and acquiring forty more points (N = 50), repeating for 1,000 MC samples. Figure 12 summarizes our results. Observe that all of REI variations outperform the others by minimizing regret faster and converging at a lower value. EI with post hoc adversary and StableOPT perform fairly well but suffer from drawbacks similar to those described in Section 4.2. They cannot accommodate squared and unsquared target locations differently.

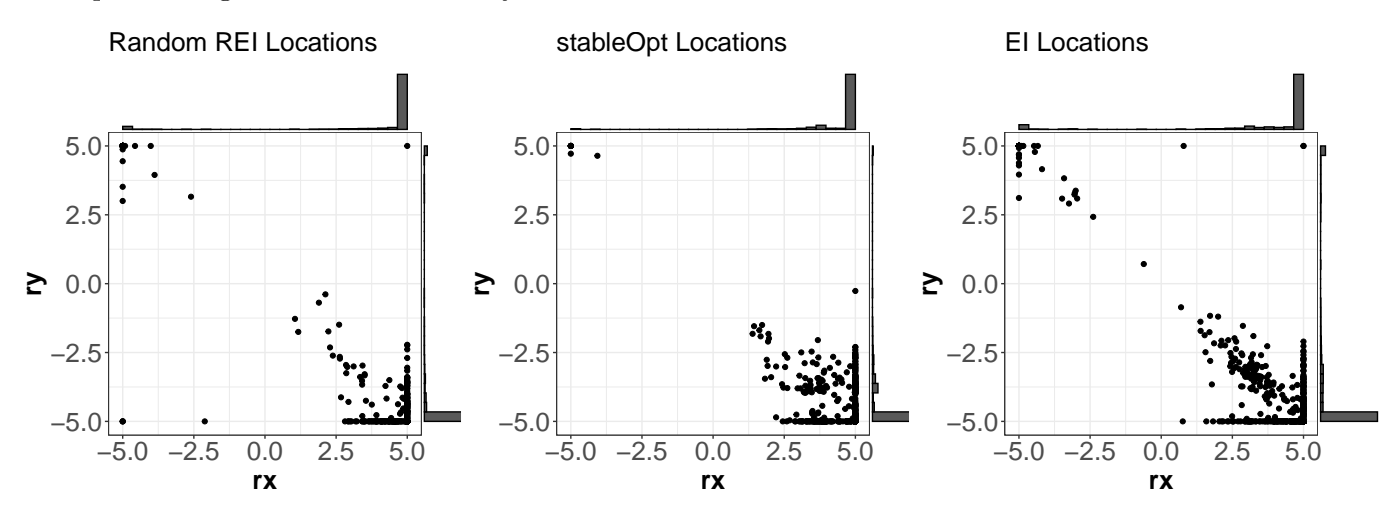


Figure 13: Distribution of r_x and r_y from x_{bear}^* for the push3 problem after the final acquisition for "rand" REI using $\alpha = 0.1$ (left), StableOPT (middle), and EI (right).

It is worth noting, that while REI performs well, the left panel of Figure 12 suggests that none of the methods are getting very close to always finding x^r when $d(x_{b,n}^*) = 0$. (Distances are not converging to zero.) To dig a little deeper, Figure 13 explores r_x and r_y from x_{bear}^* for "rand" REI, StableOPT and EI with post hoc adversary. Notice that it is rare for any of these comparators to push toward the "wrong" target location, i.e., finding (-5,5) rather than (5,-5) which would result in large $d(x_{b,n}^*)$ and low $r(x_{b,n}^*)$. However, EI is attracted to the peaked minimum more often than either of the other methods. REI has this problem slightly more often than StableOPT. However, StableOPT and EI do recommend x_{bear}^* in the bottom-right, but not all the way to (5,-5). This happens more often than with REI. Only occassionally does REI miss entirely by finding the global minimum leading to large $d(x_{b,n}^*)$. On the other hand, StableOPT identifies the correct area slightly more often, but struggles to pinpoint x^r . We conclude that both REI and StableOPT perform well – much better than ordinary EI – and any differences are largely a matter of taste or tailoring to specific use cases, modulo computational considerations (right

panel).

For "push4", the location of the robust minimum is the same in that the robot hand starts in the bottom-right, pushing to the top-left. Thus $x_r^* = (5, -5, -0.79, 25.7)$ when using $\alpha = 0.1$. Here $g(x_r^*, 0.1) = 1.64$ compared to g((-5, 5, -0.79, 25.7), 0.1) = 2.71 by pushing to the squared target location. We again compared the methods from Section 4.2 with 1,000 MC iterations, but this time with an initial LHS of size $n_0 = 20$ and eighty acquisitions (N = 100). Results are presented in Figure 14. Note that increasing the dimension makes every method do worse, but relative comparisons between methods are similar. Here StableOPT's performance is better, on par with REI variations, again modulo computing time (right panel).

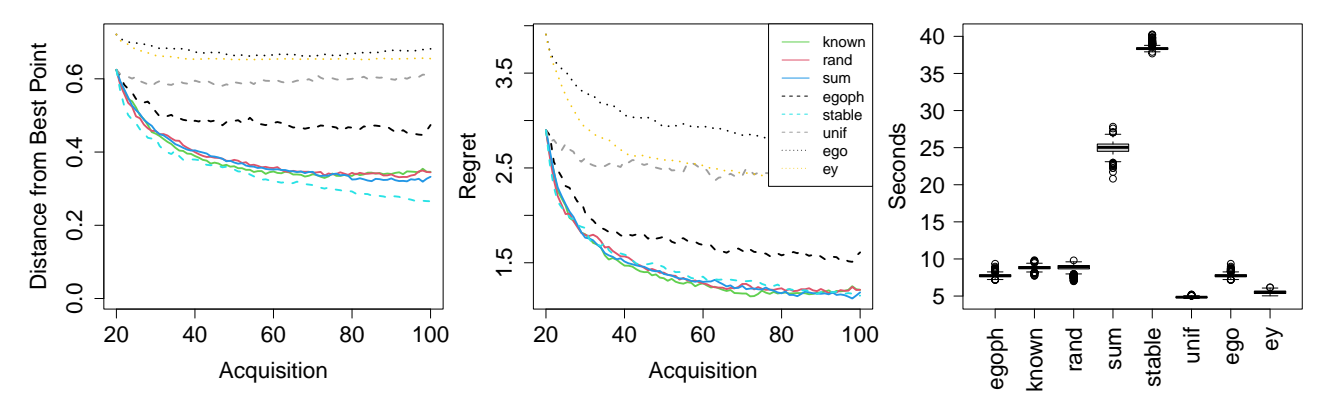


Figure 14: Results for "push4" $\alpha = 0.1$: $d(x_{\rm b,n}^*)$ (left), $r(x_{\rm b,n}^*)$ (middle) and cumulative time (right).

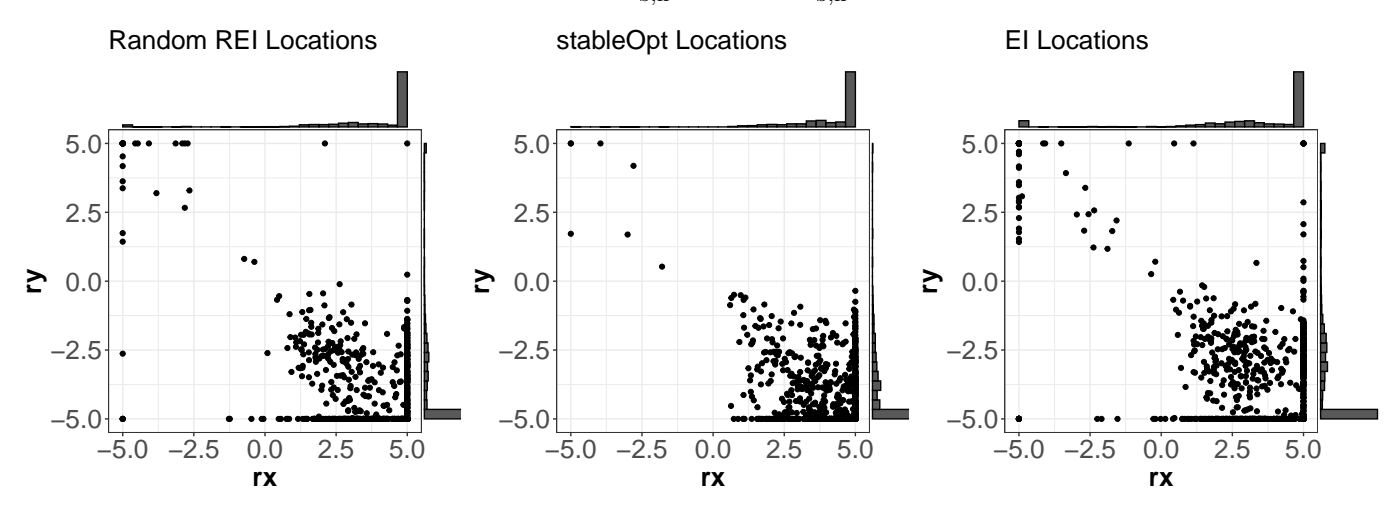


Figure 15: Distribution of r_x and r_y from x_{bear}^* for the push4 problem after the final acquisition for random REI using $\alpha = 0.1$ (left), StableOPT (middle), and EI (right).

Figure 15 demonstrates the added difficulty of the "push4" problem, as indicated by additional spread in the optimal (r_x, r_y) compared to Figure 13. This is because a slightly misspecified starting location can be compensated for by adjusting the hand angle. Incorporating that angle introduces a slew of local minima at each (r_x, r_y) . For example, if we set $r_x = 3$ rather than 5 as is optimal, and check the regret for "push3" and "push4", we get 1.1 and 0.7, respectively, by changing r_θ to -0.69. We may also adjust $t_r = 24.2$ in both cases to account for the fact the hand is closer to the box. This phenomenon is not unique to the example we chose. Any slight misspecification of r_x and r_y compensated for with a commensurate change in r_θ .

6 Discussion

We introduced a robust expected improvement (REI) criteria for Bayesian optimization (BO) that provides good experimental designs for targeting robust minima. REI is doubly robust, in a sense, because it is able to accomplish this feat even in cases where one does not know the proper level of robustness, α , to accommodate. In fact, we have shown that in some cases, not fixing the α robustness level beforehand leads to faster discovery of the robust minimum. BO methods, e.g., ordinary EI, miss the robust target entirely. However, by blending EI with an (surrogate modeled) adversary, we are able to get the best of both worlds. Even when designs are not targeted to find a robust minimum, the adversarial surrogate can be applied post hoc to similar effect.

Despite this good empirical performance, the idea of robustness undermines one of the key assumptions of GP regression: stationarity. If one optimum is peaked and another is shallow, then that surface is technically nonstationary. When there are multiple such regimes it can be difficult to pin down length-scale(s) θ , globally in the input space. The underlying REI acquisition scheme may perform even better when equipped with a non-stationary surrogate model such as the treed GP (Gramacy and Lee, 2007) or a deep GP (Damianou and Lawrence, 2013; Sauer et al., 2022). We surmise that non-GP-based surrogates, e.g., neural networks (Shahriari et al., 2020), support vector machines (Shi et al., 2020) or random forests (Dasari et al., 2019) could be substituted without a fundamental change to the underlying REI criteria.

Throughout we assumed deterministic f(x). Noise can be accommodated by estimating a nugget parameter. The idea of robustness can be extended to protect against output noise (Beland and Nair, 2017), in addition to the "input uncertainty" regime we studied here. In that setting, it can be helpful to entertain a heteroskedastic (GP) surrogate (Binois et al., 2018, 2019; Binois and Gramacy, 2019) when the noise level is changing in the input space.

Funding

This work was supported by the U.S. Department of Energy, Office of Science, Office of Advanced Scientific Computing Research and Office of High Energy Physics, Scientific Discovery through Advanced Computing (SciDAC) program under Award Number 0000231018.

References

- Abrahamsen, P. (1997). "A review of Gaussian random fields and correlation functions." Norsk Regnesentral/Norwegian Computing Center Oslo, https://www.nr.no/directdownload/917_Rapport.pdf.
- Assael, J.-A. M., Wang, Z., Shahriari, B., and de Freitas, N. (2014). "Heteroscedastic Treed Bayesian Optimisation." *ArXiv*.
- Beland, J. J. and Nair, P. B. N. (2017). "Bayesian optimisation under uncertainty." NIPS BayesOPT 2017 workshop.
- Bertsimas, D., Nohadani, O., and Teo, K. M. (2010). "Robust Optimization for Unconstrained Simulation-Based Problems." *Operations Research*, 58, 161–178.
- Binois, M. and Gramacy, R. (2019). hetGP: Heteroskedastic Gaussian process modeling and design under replication. R package version 1.1.1.
- Binois, M., Gramacy, R., and Ludkovski, M. (2018). "Practical heteroscedastic Gaussian process modeling for large simulation experiments." *Journal of Computational and Graphical Statistics*, 27, 4, 808–821.

- Binois, M., Huang, J., Gramacy, R., and Ludkovski, M. (2019). "Replication or exploration? Sequential design for stochastic simulation experiments." *Technometrics*, 27, 4, 808–821.
- Blum, A. and Mansour, Y. (2007). "Learning, Regret minimization, and Equilibria." In *Algorithmic Game Theory*, eds. N. Nisan, T. Roughgarden, E. Tardos, and V. V. Vazirani, chap. 4, 79–103. New York, NY, USA: Cambridge University Press.
- Bogunovic, I., Scarlett, J., Jegelka, S., and Cevher, V. (2018). "Adversarially Robust Optimization with Gaussian Processes." Advances in Neural Information Processing Systems, 31, 5760–5770.
- Box, G. and Draper, N. (2007). Response Surfaces, Mixtures, and Ridge Analyses, vol. 649. John Wiley & Sons.
- Burden, R. L. and Faires, J. D. (1989). *Numerical Analysis*. The Prindle, Weber and Schmidt Series in Mathematics, 4th ed. Boston: PWS-Kent Publishing Company.
- Byrd, R. H., Lu, P., Nocedal, J., and Zhu, C. (1995). "A Limited Memory Algorithm for Bound Constrained Optimization." SIAM Journal on Scientific Computing, 16, 5, 1190–1208.
- Catto, E. (2011). "Box2D, a 2D physics engine for games."
- Cheney, E. W. and Goldstein, A. A. (1959). "Newton's Method for Convex Programming and Tchebycheff Approximation." *Numer. Math.*, 1, 1, 253–268.
- Damianou, A. and Lawrence, N. D. (2013). "Deep Gaussian Processes." In *Proceedings of the Sixteenth International Conference on Artificial Intelligence and Statistics*, eds. C. M. Carvalho and P. Ravikumar, vol. 31 of *Proceedings of Machine Learning Research*, 207–215. Scottsdale, Arizona, USA: PMLR.
- Dasari, S. K., Cheddad, A., and Andersson, P. (2019). "Random Forest Surrogate Models to Support Design Space Exploration in Aerospace Use-Case." In *Artificial Intelligence Applications and Innovations*, eds. J. MacIntyre, I. Maglogiannis, L. Iliadis, and E. Pimenidis, 532–544. Cham: Springer International Publishing.
- Dean, A., Morris, M., Stufken, J., and Bingham, D. (2015). *Handbook of Design and Analysis of Experiments*. Chapman & Hall/CRC Handbooks of Modern Statistical Methods. CRC Press.
- Dixon, L. C. W. and Szego, G. P. (1979). The global optimization problem: an introduction. Amsterdam: North-Holland Pub. Co.
- Gramacy, R. B. (2016). "laGP: Large-Scale Spatial Modeling via Local Approximate Gaussian Processes in R." *Journal of Statistical Software*, 72.
- (2020). Surrogates: Gaussian Process Modeling, Design and Optimization for the Applied Sciences. Boca Raton, Florida: Chapman Hall/CRC.
- Gramacy, R. B. and Lee, H. K. H. (2007). "Bayesian treed Gaussian process models with an application to computer modeling."
- Gramacy, R. B., Sauer, A., and Wycoff, N. (2022). "Triangulation candidates for Bayesian optimization."
- Hong, L. and Nelson, B. (2006). "Discrete optimization via simulation using COMPASS." *Operations Research*, 54, 115–129.

- Huang, L., Joseph, A., Nelson, B., Rubinstein, B. I. P., and Tygar, J. (2011). "Adversarial machine learning." In *AISec '11*, ed. Y. Chen.
- Jones, D., Schonlau, M., and Welch, W. (1998). "Efficient Global Optimization of Expensive Black-Box Functions." *Journal of Global Optimization*, 13, 455–492.
- Kaelbling, L. and Lozano-Perez, T. (2017). "Learning composable models of parameterized skills." 886–893.
- Kaelbling, L. P., Littman, M. L., and Moore, A. W. (1996). "Reinforcement learning: A survey." *Journal of Artificial Intelligence Research*, 4, 237–285.
- Kalpić, D. and Hlupić, N. (2011). *Multivariate Normal Distributions*, 907–910. Berlin, Heidelberg: Springer Berlin Heidelberg.
- Martinez-Cantin, R., Freitas, N., Brochu, E., Castellanos, J., and Doucet, A. (2009). "A Bayesian exploration-exploitation approach for optimal online sensing and planning with a visually guided mobile robot." *Auton. Robots*, 27, 93–103.
- Marzat, J., Walter, E., and Piet-Lahanier, H. (2016). "A new expected-improvement algorithm for continuous minimax optimization." J. Glob. Optim., 64, 4, 785–802.
- Menickelly, M. and Wild, S. M. (2020). "Derivative-Free Robust Optimization by Outer Approximations." *Mathematical Programming*, 179, 1–2, 157–193.
- Mockus, J., Tiesis, V., and Zilinskas, A. (1978). "The application of Bayesian methods for seeking the extremum." *Towards Global Optimization*, 2, 117-129, 2.
- Myers, R., Montgomery, D., and Anderson-Cook, C. (2016). Response Surface Methodology: Process and Product Optimization Using Designed Experiments. John Wiley & Sons.
- Neal, R. (1998). "Regression and classification using Gaussian process priors." Bayesian Statistics, 6, 475.
- Nogueira, J., Martinez-Cantin, R., Bernardino, A., and Jamone, L. (2016). "Unscented Bayesian Optimization for Safe Robot Grasping." *CoRR*, abs/1603.02038.
- Oliveira, R., Ott, L., and Ramos, F. (2019). "Bayesian optimisation under uncertain inputs." In *Proceedings* of the Twenty-Second International Conference on Artificial Intelligence and Statistics, eds. K. Chaudhuri and M. Sugiyama, vol. 89 of Proceedings of Machine Learning Research, 1177–1184. PMLR.
- R Core Team (2021). R: A Language and Environment for Statistical Computing. R Foundation for Statistical Computing, Vienna, Austria.
- Randall, S. E., Halsted, D. M., I., and Taylor, D. L. (1981). "Optimum Vibration Absorbers for Linear Damped Systems." *Journal of Mechanical Design*, 103, 4, 908–913.
- Rasmussen, C. and Williams, C. (2006). Gaussian Processes for Machine Learning. Cambridge, MA: MIT Press.
- Sacks, J., Welch, W. J., Mitchell, T. J., and Wynn, H. P. (1989). "esign and Analysis of Computer Experiments." *Statistical Science*, 4, 409–423.
- Santner, T., Williams, B., and Notz, W. (2018). The Design and Analysis of Computer Experiments, Second Edition. New York, NY: Springer-Verlag.

- Sauer, A., Cooper, A., and Gramacy, R. B. (2022). "Vecchia-approximated Deep Gaussian Processes for Computer Experiments."
- Scott, W., Frazier, P., and Powell, W. (2011). "The Correlated Knowledge Gradient for Simulation Optimization of Continuous Parameters using Gaussian Process Regression." SIAM Journal on Optimization, 21, 996–1026.
- Shahriari, B., Swersky, K., Wang, Z., Adams, R. P., and de Freitas, N. (2016). "Taking the Human Out of the Loop: A Review of Bayesian Optimization." *Proceedings of the IEEE*, 104, 1, 148–175.
- Shahriari, M., Pardo, D., Moser, B., and Sobieczky, F. (2020). "A Deep Neural Network as Surrogate Model for Forward Simulation of Borehole Resistivity Measurements." *Procedia Manufacturing*, 42, 235–238. International Conference on Industry 4.0 and Smart Manufacturing (ISM 2019).
- Shi, M., Lv, L., Sun, W., and Song, X. (2020). "A Multi-Fidelity Surrogate Model Based on Support Vector Regression." Struct. Multidiscip. Optim., 61, 6, 2363–2375.
- Snoek, J., Larochelle, H., and Adams, R. P. (2012). "Practical Bayesian optimization of machinelearning algorithms." Advances in Neural information Processing Systems (NIPS), 2951–2959.
- Stein, M. L. (1999). Interpolation of spatial data. Springer-Verlag.
- Taddy, M. A., Lee, H. K. H., Gray, G. A., and Griffin, J. D. (2009). "Bayesian Guided Pattern Search for Robust Local Optimization." Technometrics, 51, 4, 389–401.
- Vanchinathan, H. P., Nikolic, I., De Bona, F., and Krause, A. (2014). "Explore-Exploit in Top-N Recommender Systems via Gaussian Processes." In *Proceedings of the 8th ACM Conference on Recommender Systems*, eds. A. Kobsa and M. Zhou, RecSys '14, 225–232. Association for Computing Machinery.
- Wang, Z. and Jegelka, S. (2017). "Max-Value Entropy Search for Efficient Bayesian Optimization." In Proceedings of the 34th International Conference on Machine Learning Volume 70, ICML'17, 3627–3635. JMLR.org.
- Wang, Z., Li, C., Jegelka, S., and Kohli, P. (2017). "Batched High-dimensional Bayesian Optimization via Structural Kernel Learning." In *Proceedings of the 34th International Conference on Machine Learning*, eds. D. Precup and Y. W. Teh, vol. 70 of *Proceedings of Machine Learning Research*, 3656–3664. PMLR.
- Zhang, B., Cole, D., and Gramacy, R. (2020). "Distance-distributed design for Gaussian process surrogates." To appear in Technometrics. Preprint on arXiv:1812.02794.